Theoretical consideration of fallout particles formation in case of atmospheric nuclear explosion and assessment of deposition density due to Hiroshima "black rain"

E.O. Granovskaya[1], G.A. Krasilov[2], S.M. Shinkarev[1], V.N. Yatsenko[1], M. Hoshi[3].

[1]*Burnasyan Federal Medical Biophysical Center, Moscow, Russia*

[2] *Institute of Global Climate and Ecology, Moscow, Russia*

[3]*Research Institute for Radiation Biology and Medicine, University of Hiroshima, Hiroshima, Japan*

On August 6, 1945 an A-bomb "Little Boy" exploded above Hiroshima. In about 20 minutes it began to rain from the radioactive cloud. The rain drops were black and big as balls [1]. The cloud moved north-west from the hypocenter. Precipitations from the radioactive cloud covered the area of about 66 km^2 hereinafter referred to as the "black rain" area.

Since 2008 joint international efforts to assess doses to Hiroshima residents due to the "black rain" have been under way. One of the central problems relating to dose assessment is estimation of qualitative and quantitative composition of fallout deposition. So, the purpose of this work is to reconstruct a realistic radioactive contamination of the "black rain" area on the basis of known theoretical statements, analysis of a few experimental measurements and plausible thoughts.

Three tasks have been set:

1) reconstruction of radioactive particles formation in case of an atmospheric nuclear explosion;

2) estimation of the radionuclides deposition density due to Hiroshima "black rain";

3) preliminary assessment of external doses due to radionuclides deposited on the ground in the "black rain area".

Reconstruction of radioactive particles formation in case of an air nuclear explosion

An air nuclear explosion that has the reduced height of burst more than 100 $m/kt^{1/3}$ is called "air explosion". Under these conditions the expanding fireball doesn't touch the ground surface. Hence, no soil is involved in the fireball. In this case a single-phase multi-component thermodynamic system, formed in the fireball soon after the explosion, consists of device construction materials vapors, nuclear fuel, fission products and device-related activation products and hot air. Then the fireball begins to cool down. It inevitably leads to vapors condensation resulting in creation of the liquid phase in the form of ferrous oxide drops because ferrum is the main construction material of the device. While drops are growing, molecules of radionuclides are condensing on these drops in accordance with their thermodynamic properties. This process continues till the drops have solidified and changed into spherical solid particles with practically uniform volume distribution of radionuclides.

To obtain numerical results a two-phase multi-component vapor-liquid system in thermodynamic equilibrium was considered. This system can be described using several assumptions. The first assumption: the processes, which progress in both phases of the system, can be considered as

combination of consecutive short-time events. All equilibrium conditions are kept in every event (so-called quasi-thermodynamic equilibrium principle). The second assumption: the liquid phase, which is a combination of great amount of different size spherical drops, is a highly diluted multi-component solution, which behaves as an ideal solution. The third assumption: vapors of solvent and soluble behave as ideal gases.

We can break the process of fallout particles formation into several intervals according to the fireball temperature.

The first interval: $T > 1641$ °K. Under this condition vapor phase molecules interact with liquid drops of ferrous oxide. Consolidation of the drops totally finishes by T = 1641 °K. Within the frame of this interval behavior of radionuclides in the fireball could be described according to one of kinetic interpretations of Henry law. Firstly, radionuclides of refractory elements and their oxides formed till consolidation of the liquid drops are concentrated in the volume of these drops. Secondly, most of radionuclides of halogens, noble gases and volatile elements, such as rubidium and cesium, remain in vapor phase.

The second interval: $373°K < T < 1641°K$. The radionuclides remained in vapor phase or newly formed according to the corresponding decay chains are adsorbed on the surface of the solidified drops in accordance with Langmur physical adsorption theory.

Langmur's assumptions were as follows:

- there is a certain quantity of adsorption sites on solid body (adsorbent) surface. Vapor phase molecules can be adsorbed on these sites;
- adsorption site is an atom or a molecule of adsorbent, which possesses an unsaturated bond. This bond creates force field. It should be noted that each adsorption site is able to capture and to keep on its surface for some time one and only one strange molecule which has entered its force field;
- adsorption sites are equivalent, each adsorbed molecule is equally strongly bonded to the adsorbent. Surface migration of the adsorbed molecule is impossible.

In case of equilibrium between isobars adsorbed on the particles surface and isobars remained in vapor phase only a part of adsorption sites is occupied.

Isobars of decay chains involve wide range of compounds from noble gases and halogens to refractory metallic oxides. Their behavior in the fireball after consolidation of the particles depends on their thermodynamic properties. Firstly, time of residence on the particles surface of refractory isobar molecules is rather large and the probability of their sorption is close to 1. Secondly, radionuclides of volatile and intermediate elements are partly adsorbed on the particles surface. Thirdly, sorption of noble gases on the surface of condensation particles is improbable. Finally, radionuclides not related to the particles are presented as a part of aerosols and form global fallout.

The third interval: $T < 373°K$. By this moment adsorption of the radionuclides practically finishes. Intensive condensation of atmospheric moisture vapors begins. Then this moisture evaporates or sublimates resulting in loose aerosols.

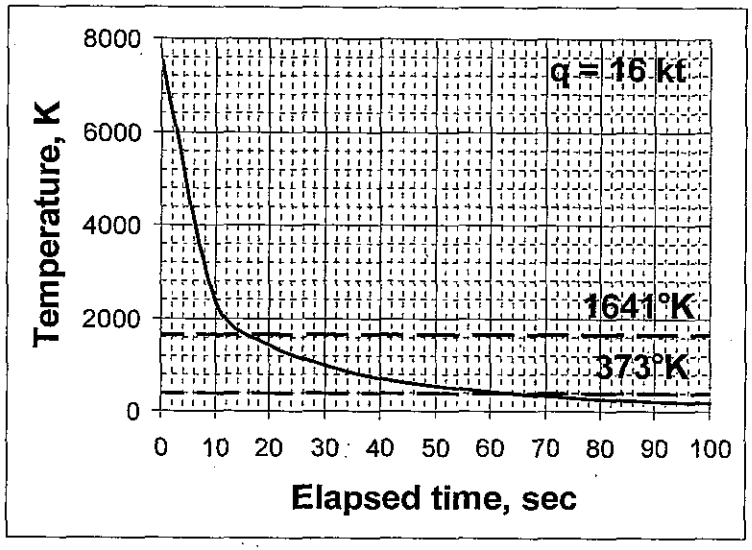

Fig. 1 Temperature of the fireball versus time.

According to Fig.1 we can conclude that consolidation of drops finishes in about 15 seconds after the explosion and formation of fallout particles finishes in about one minute after the explosion.

Estimation of the radionuclides deposition density due to Hiroshima "black rain"

Several assumptions have been made in order to estimate the deposition density. They are as follows:

- the "black rain" began just after the explosion;
- fission yield of the explosion "Little Boy" was equal to 16 kt;
- the "black rain" area was equal to 66 km^2;

To assess deposition density we need to estimate the fraction of the nuclear explosion particles deposited in the "black rain" area.

The ^{238}U surface density in the "black rain" area is mainly determined by natural uranium and it is equal to *phk*:

ρ – soil density at the soil sampling point, g·cm^{-3};

h – soil depth in the case of the standard sampling, which is equal to 10 cm;

k – relative mass content of natural uranium in soil at the soil sampling point.

The ^{236}U deposition density can be written as: $\frac{\alpha \cdot m_{236}}{S}$

α – the fraction of the nuclear explosion particles deposited in the "black rain" area;

S – the "black rain" area, which is equal to 66 km^2.

Then, $\frac{^{236}U}{^{238}U} = \frac{\alpha \cdot m_{236}}{S} \cdot \frac{1}{\rho \cdot h \cdot k} = \frac{m_{236}}{\rho \cdot h \cdot S} \cdot \frac{\alpha}{k}$ (1)

Let's assume that energy release of the A-bomb "Little Boy" was 16 kt in TNT equivalent. Taking into account that there are 1.45 10^{23} fissions per 1 kt, we can assess that 2.32 10^{24} atoms or ~905g of ^{235}U were fissioned.

The ratio between radioactive-capture cross-section and fission cross-section is equal to 0.0738. Hence, during nuclear fission 0.0738·2.32 10^{24}=1.71 10^{23} atoms or 67.1g of ^{236}U were formed as a result of radioactive capture. So, m_{236} = 67.1 g.

$\frac{^{236}U}{^{238}U}$ -is an experimental ratio which characterizes the soil sampling point.

We can estimate the magnitude of the $\frac{\alpha}{k}$ using equation (1) and experimental data [2]. It fairly characterizes a certain average value for the "black rain" area. In accordance with the calculations,

$\frac{\bar{\alpha}}{k}$ =2658.

Uranium is a rock-forming but rather trace element. The clarke content of natural uranium is equal to 3 10^{-6}. However, density of natural uranium essentially depends upon a kind of rock, so it can vary over rather a wide range. Therefore k depends upon composition of the rock, which forms sub-base at the sampling point. Assuming k is equal to the clarke of natural uranium, we obtain that $\alpha = 2658 \cdot 3 \cdot 10^{-6} \approx 0.8\%$.

Values of surface contamination density were calculated using the following formula:

$$\sigma_j = \frac{\varphi_j \cdot 1.45 \cdot 10^{23} \cdot q \lambda_j \frac{N_j}{N_{t_j}} \alpha}{3.7 \cdot 10^{10} \cdot S}, \quad (2)$$

where: φ_j - independent yield of j-th isobar decay chain in case of ^{235}U fission by fission spectrum neutrons;

1.45 10^{23} fissions per kt - amount of fissions which corresponds to the fission yield of 1 kt;

q – fission yield of the explosion "Little Boy" which is equal to 16 kt;

λ_j -decay constant of the main isobar of j-th decay chain,s^{-1};

$\frac{N_j}{N_{t_j}}$ - the fraction of j-th decay chain isobars which relates to the nuclear explosion particles (according to our estimate);

α – the fraction of the nuclear explosion particles deposited in the "black rain" area, which is equal to 0.8%;

3.7 10^{10} - decays per second to Ci conversion coefficient;

S - the "black rain" area, which is equal to 66 km^2.

The values of independent yields of isobar decay chains were copied from the guide [3] and the values of decay constants were calculated using data presented in the guide [4].

Values of ratio $\frac{N_j}{N_{t_j}}$ for the series of isobar decay chains which take place in case of an atmospheric atomic explosion with fission yield of about 20 kt and average values of fission fragments contamination density of the "black rain" fallout are presented in Table 1.

Table 1

The decay chain number	The main radionuclide	$T_{1/2}$	$\frac{N_j}{N_{t_j}}$	σ, kBq/m^2
89	^{89}Sr	50.55 d	0.0023	4.44
90	^{90}Sr	28.6 y	0.012	0.11
91	^{91}Y	58.51 d	0.056	1.15 10^2
95	^{95}Zr	64.05 d	1	2.4 10^3
	^{95}Nb	34.97 d	1	
99	^{99}Mo	66.02 h	0.94	4.81 10^4
103	^{103}Ru	39.35 d	0.44	1 10^3
106	^{106}Ru	368.2 d	0.29	8.51
131	^{131}I	8.04 d	0.42	3.71 10^3
132	^{132}Te	78.2 h	0.45	1.4 10^4
	^{132}I	2.3 h	0.45	
137	^{137}Cs	30.174 y	0.015	0.19
140	^{140}Ba	12.789 d	0.28	2.8 10^3
	^{140}La	1.68 d	0.28	
141	^{141}Ce	32.5 d	0.62	2.3 10^3
143	^{143}Ce	33.0 h	1	9.6 10^2
144	^{144}Ce	284.31 d	1	5.9 10^2

Based on our results we can make some conclusions: 1) Condensation particles mainly are the cause of radioactive contamination in intermediate fallout zones; 2) Such radionuclides as ^{90}Sr and ^{137}Cs are predominantly condensed on the atmospheric dust particles and aerosols and form the basis of global fallout; 3) Qualitative and quantitative composition of radioactive contamination of air explosion particles depend upon a nuclear explosion yield.

Preliminary assessment of external doses due to radionuclides deposited on the ground in the "black rain" area

We have obtained deposition density of different radionuclides in the "black rain" area. Hence, we can assess external doses due to the "black rain". Preliminary estimates of external doses for the first year after deposition from different radionuclides are presented in Table 2.

Table 2. Preliminary estimates of external doses.

Radionuclide	External absorbed dose, mGy y^{-1}
^{89}Sr	2.64 10^{-2}
^{91}Y	3 10^{-3}
^{95}Zr/^{95}Nb	14.5
^{99}Mo	2.4
^{103}Ru	2.6
^{131}I	1.45
^{132}Te	14.2
^{137}Cs	4 10^{-3}
^{140}Ba/^{140}La	9.3
^{141}Ce	0.7
^{143}Ce	5.4 10^{-2}
^{144}Ce	0.23

According to our calculations the preliminary maximum estimate of the external dose accumulated during one year after the explosion from all deposited fallout particles to the residents in the "black rain" area is about 46 mGy.

Main conclusions are as follows:

1. The process of radioactive particles formation in case of an air nuclear explosion has been reconstructed step-by-step.
2. Quick fractionation of the radionuclides took place in case of Hiroshima "black rain". Mixture of deposited particles was depleted with such radionuclides as ^{89}Sr, ^{90}Sr, ^{91}Y and ^{137}Cs.
3. Radionuclides not related to the particles were condensed on the atmospheric dust particles and loose aerosols.
4. The deposition density of various radionuclides due to Hiroshima 'black rain" has been estimated.
5. Condensation particles mainly are the cause of radioactive contamination in intermediate fallout zones.
6. Only small amount of fission products was deposited in the "black rain" area. Such radionuclides as ^{90}Sr and ^{137}Cs were depleted in fallout particles. The major part of fission particles was globally deposited.
7. Qualitative and quantitative composition of radioactive contamination of fallout particles depend upon conditions and yield of a nuclear explosion.
8. The preliminary maximum estimate of the external dose from all deposited fallout particles to the residents in the "black rain" area is about 46 mGy.

REFERENCES

1. E.A. Melvin-Hughes, Physical Chemistry (Russian translation), Vol.2, Izd. Inostr. Lit., Moscow 1962
2. T. Imanaka. Private communication
3. M.P. Grechushkina Tables of instantaneous fission products composition for U-235, U-238, Pu-239 Atomizdat Moscow 1964
4. N.G. Gusev, P.P. Dmitriev Radioactive chains. Atomizdat Moscow 1978

Methodology on estimation of internal dose due to Hiroshima "black rain"

E.O. Granovskaya[1], S.M. Shinkarev[1], G.A. Krasilov[2], V.N. Yatsenko[1], M. Hoshi[3]

[1]*Burnasyan Federal Medical Biophysical Center, Moscow, Russia*

[2] *Institute of Global Climate and Ecology, Moscow, Russia*

[3]*Research Institute for Radiation Biology and Medicine, University of Hiroshima, Hiroshima, Japan*

On August 6, 1945 an A-bomb exploded above Hiroshima. Shortly it began to rain from the radioactive cloud. The cloud moved north-west from the hypocenter. Precipitations from the radioactive cloud covered the area of about 66 km^2, so-called the "black rain" area. Deposited radionuclides could be the cause of external and internal exposure to the Hiroshima residents. The purpose of this work is to present the method of reconstruction of internal doses to critical organs for the inhabitants of the "black rain" area.

In 2000 the methodology "Assessment of absorbed and effective doses from ionizing radiation to the populations living in areas of local fallout from atmospheric nuclear explosions" was developed by Russian scientists (K.I. Gordeev and colleagues) [1]. This methodology has been adapted to the Hiroshima "black rain" fallout conditions. Also the paper by H. Muller and G. Prohl "ECOSYS-87: a dynamic model for assessing radiological consequences of nuclear accidents" [2] was used. The resulting methodology is described.

The main input parameters related to the nuclear explosion were as follows: 1) date of the explosion: August 6, 1945; 2) type and composition of fission material: $^{235}U \sim 80\%$, $^{234}U \sim 3\%$, $^{238}U \sim 17\%$; 3) total yield of the explosion: $q \approx 16$ kt in TNT equivalent.

We have made several assumptions related to residence history and dietary habits: 1) the inhabitants permanently lived in the "black rain" area at the time of the explosion and at least a year following it; 2) diet wasn't changed after the deposition.

Absorbed dose in organ to age-group k from internal exposure of radionuclide i ($D_{int,i,k}$) is equal to the sum of dose from inhaled nuclide i ($D_{inh,i,k}$) and dose from ingested nuclide i ($D_{ing,i,k}$):

$$D_{int,i,k} = D_{inh,i,k} + D_{ing,i,k} \quad (1)$$

Let's consider internal dose from inhaled nuclide i. It is directly-proportional to the integral concentration of nuclide i in air, which in its turn depends upon deposition velocity of nuclide i:

$$D_{inh,i,k} \sim C_\infty = \frac{\sigma}{V_d} \quad (2)$$

where

C_∞ is integral concentration of nuclide i in air;

σ is deposition density of nuclide i;

V_d is deposition velocity of nuclide i.

In case of dry deposition $V_d \approx 0.1\text{-}0.3$ m s^{-1}, while in case of wet deposition $V_d \approx 5\text{-}10$ m s^{-1}. So we can conclude that in case of wet deposition internal dose due to inhalation is ~ 100 times less than that in case of dry deposition. It's well known that usually (in case of dry deposition) the contribution to total internal dose from inhalation intake is much less than that from ingestion intake. Hence, we can assume that in case of Hiroshima, where wet deposition took place, internal dose has been totally determined with the dose from ingestion intake:

$$D_{int,i,k} \cong D_{ing,i,k} \quad (3)$$

Let's consider internal dose from ingestion of radionuclides. The first task is to determine the main route of intake. We have results of some interviews of Hiroshima residents regarding typical diet in 1945, which was kindly furnished by Professor M. Hoshi. We have carefully analyzed it and made the following conclusions: 1) Consumption of leafy vegetables was less than in case of Chernobyl and Semipalatinsk. So we can neglect this route of intake; 2) For the Hiroshima residents the goat's (not cow's) milk was determined as typical. Furthermore, it's well known that concentration of ^{131}I in goat's milk is 5-7 higher than that in cow's milk. We can conclude that intake of radionuclides with goat's milk was predominant. It should be noted that it is correct only for those people who used to drink goat's milk. On the basis on the foregoing the internal dose from ingestion of nuclide i can be written as follows:

$$D_{ing,i,k} = DF_{ing,i,k} \times V_{m,k} \times \int_0^{t_2} C_{m,i}(t)dt / p_{m,i,k} \quad (4)$$

where

$DF_{inh,i,k}$ is age-dependent organ dose factor from ingestion of i-th nuclide, Gy Bq^{-1};

$V_{m,k}$ is age-dependent milk consumption rate, L d^{-1};

$C_{m,i}(t)$ is concentration of i-th nuclide in milk, Bq L^{-1};

t_2 is time limit for integration, d;

$p_{m,i,k}$ is age-dependent fraction of intake of nuclide i with milk in the entire intake, dimensionless.

To assess concentration of nuclide i in milk we need to know concentration of this nuclide in pasture grass.

Total intake of ^{131}I is determined by ingestion intake during the first two months after the explosion. Taking into account the Chernobyl experience, the ingestion intake of ^{137}Cs and ^{90}Sr during the first two months after the explosion is about 10% of lifetime dose. So, we will consider internal doses due to ^{137}Cs and ^{90}Sr intake during two months in order to make an estimate of total lifetime dose. It is worth noting that the concentration of ^{137}Cs and ^{90}Sr in pasture grass during the first two months is mainly determined by aerial contamination of pasture vegetation.

It was an air explosion. Consequently the size of the fallout particles didn't exceed 10-25 microns and the average size was less than 1 micron. Hence, all fallout particles were related to biologically active fraction and were readily retained by the pasture grass. Equation to assess the concentration of nuclide i in grass can be written as follows:

$$C_{gr,i}(t) = (\sigma_i/Y) \times \exp(-(\lambda_{gr,i}+\lambda_i) \times t) \quad (5)$$

where

σ_i is deposition density of the i-th nuclide in the "black rain" area, Bq m^{-2};

Y is yield of pasture grass in the "black rain" area, kg m^{-2};

$\lambda_{gr,i}$ is weathering removal rate of the i-th radionuclide from pasture grass, d^{-1};

λ_i is radioactive decay constant for the i-th nuclide, d^{-1};

t is time counted from the date of the explosion, d.

Now we can write an equation to assess concentration of nuclide i in milk:

$$C_{m,i}(t) = \beta_i \times TF_{m,i} \times \sum_{j=1}^{N} A_{j,i} \times \int_0^t C_{gr,i}(\tau) \times Q_f \times \lambda_{cj,i} \times e^{-(\lambda_{cj,i}+\lambda_i)\times(t-\tau)} d\tau \quad (6)$$

where

$TF_{m,i}$ is feed-to-milk transfer factor for i-th nuclide, d L^{-1};

Q_f is daily intake rate of pasture grass by goat, kg d^{-1} wet;

$A_{j,i}$ and $\lambda_{cj,i}$ are empirical constants related to biological removal rate of nuclide i from goat's milk;

N=1 (one component model) for ^{131}I and N=2 (two component model) for ^{137}Cs, ^{90}Sr

β_i is solubility of nuclide i in the fallout particles;

λ_i is radioactive decay constant for the i-th nuclide, d^{-1};

When internal dose is defined by ingestion intake, the following cases should be considered: 1) internal dose to thyroid from ^{131}I; 2) internal dose to red marrow from ^{90}Sr; 3) internal dose to whole body from ^{137}Cs. Hence, we need to know concentration of ^{131}I, ^{90}Sr and ^{137}Cs in goat's milk.

The equation to assess the time-integrated concentration of ^{131}I in milk during two months, $C_{m,131}(0 - t_2)$, can be written as follows:

$$C_{m,131}(0 - t_2) = C_{m,131}(0 - \infty) = X_0/X_1 \quad (7)$$

where

$X_0 = \beta_I \times TF_{m,I} \times (\sigma_I/Y) \times Q_f \times \lambda_{c,I}$;

$X_1 = (\lambda_{gr,I} + \lambda_{131}) \times (\lambda_{c,I} + \lambda_{131})$;

$t_2 = 2$ months.

The equation to assess the concentration of ^{137}Cs and ^{90}Sr in milk, $C_{m,i}(t)$, can be written as follows [Muller and Prohl, 1993]:

$$C_{m,i}(t) = \beta_i \times TF_{m,i} \times \sum_{j=1}^{2} A_{j,i} \times \int_0^t C_{gr,i}(\tau) \times Q_f \times \lambda_{cj,i} \times e^{-\lambda_{cj,i}\times(t-\tau)} d\tau \quad (8)$$

For cesium:

$A_{1,Cs}=0.8$ and $A_{2,Cs}=0.2$, dimensionless;

$\lambda_{c1,Cs}=0.46$ d^{-1} and $\lambda_{c2,Cs}=0.046$ d^{-1} are biological removal rates of cesium from goat to goat's milk, corresponding to A_1 and A_2, respectively, d^{-1}.

For strontium:

$A_{1,Sr}=0:9$ and $A_{2,Sr}=0.1$, dimensionless;

$\lambda_{c1,Sr}=0.23$ d^{-1} and $\lambda_{c2,Sr}=0.007$ d^{-1} are biological removal rates of strontium from goat to goat's milk, corresponding to A_1 and A_2, respectively, d^{-1}.

The equation (8) can be written as follows:

$$C_{m,i}(0\text{-}t_2) = W_{0,i} \times (W_{1,i} + W_{2,i}) \quad (9)$$

where

$W_{0,i} = \beta_i \times f_{m,i} \times C_{gr,i}(0) \times Q_f$

$W_{1,i} = A_{1,i} \times \lambda_{c1,i} / (\lambda_{c1,i} - \lambda_{gr,i}) \times (Z_0 - Z_1)$

$W_{2,i} = A_{2,i} \times \lambda_{c2,i} / (\lambda_{c2,i} - \lambda_{gr,i}) \times (Z_0 - Z_2)$

$Z_0 = [1\text{-}\exp(-\lambda_{gr,i} \times t_2)] / \lambda_{gr,i}$

$Z_1 = [1\text{-}\exp(-\lambda_{c1,i} \times t_2)] / \lambda_{c1,i}$

$Z_2 = [1\text{-}\exp(-\lambda_{c2,i} \times t_2)] / \lambda_{c2,i}$

$t_2 = 2$ months.

According to our assessment the preliminary estimate of internal dose to thyroid from ^{131}I for children of about 1 year who constantly consumed 0.3 L d^{-1} of goat's milk in case of maximum solubility of ^{131}I in fallout particles can be up to 1 Gy.

Main conclusions are as follows:

1. Due to the fact that wet deposition took place in the "black rain" area, the contribution to the total internal dose from inhalation intake can be neglected. So, internal dose has been totally determined with the dose from ingestion intake.
2. According to analysis of Hiroshima inhabitants typical diet, the main intake route was ingestion of radionuclides with goat's milk.
3. Ingestion intake of ^{131}I, ^{137}Cs and ^{90}Sr during the first two months after the explosion has been considered. Hence only aerial contamination of pasture grass should be considered to assess concentration of nuclide i in pasture grass.
4. All fallout particles were related to biologically active fraction and were readily retained by the pasture grass.
5. According to our assessment preliminary estimate of internal dose to thyroid from ^{131}I for children about 1 year who constantly consumed goat's milk in case of maximum solubility of ^{131}I in fallout particles can be up to 1 Gy.

REFERENCES

1. K. Gordeev et al. Assessment of absorbed and effective doses from ionizing radiation to the populations living in areas of local fallout from atmospheric nuclear explosions. Methodical guidance MU 2.6.1.1001-00. Official publication. Ministry of Public Health of the RF, Sanitary State Service of the RF, Moscow. 2000 (in Russian)
2. H. Muller and G. Prohl. ECOSYS-87: a dynamic model for assessing radiological consequences of nuclear accidents. Health Phys. 1993 Mar;64(3):232-52

On the unusual distribution of Pu/Cs activity ratios in Hiroshima soils. Can they be used to locate Black Rain sites?

N.E.Whitehead[1], M.Yamamoto[2], A. Sakaguchi[3] and M. Hoshi[1]

[1]*Research Institute of Radiation Biology and Medicine, Hiroshima University, Hiroshima*
[2]*Low Level Radiation Laboratory, Kanazawa University, Kanazawa*
[3]*Faculty of Science, Hiroshima University, Higashi-Hiroshima.*

Abstract. The previous conclusions of authors are confirmed: One cannot use by present methods, ^{137}Cs analyses alone, to detect fallout due to the Black Rain. Work by Yamamoto et al. (1985) also showed that no soils he analysed for ^{239,240}Pu and ^{137}Cs could be used to detect sites of black rain. The present paper greatly extends that analysis with many more points and confirms that the Pu/Cs ratio still cannot be used to detect black rain by current methods. In passing it is shown that the ^{137}Cs results of Hashizume et al. (1978) are systematically too low compared with analyses of the same soils by Yamamoto et al. When this correction is made it is found that the resulting data points cannot be distinguished from global fallout. It is calculated that the Pu/Cs ratio from the Hiroshima bomb would have had a value of 0.00055, and the lowest result in the data series is about 0.01 – much higher. There is therefore no trace of local Hiroshima fallout detected – it is hidden by the large amounts of later fallout from global testing. The likely chemistry of black rain is surveyed and it is concluded that the carbon created could have had many of the characteristics of activated carbon and absorb many of the radionuclides which normally would stay volatile. This would be a possible explanation if the refractory/volatile ratios in soils and wall streaks differ from those found from other fallout in soils.

^{137}Cs is not a good sole indicator of black rain

According to (Shizuma et al. 1996) (following early collection by Nishina) the ^{137}Cs in soil at Hiroshima collected soon after the explosion was much less than the subsequent global fallout from nuclear weapons testing. The contrast is shown in Fig. 1. This means the task is very difficult.

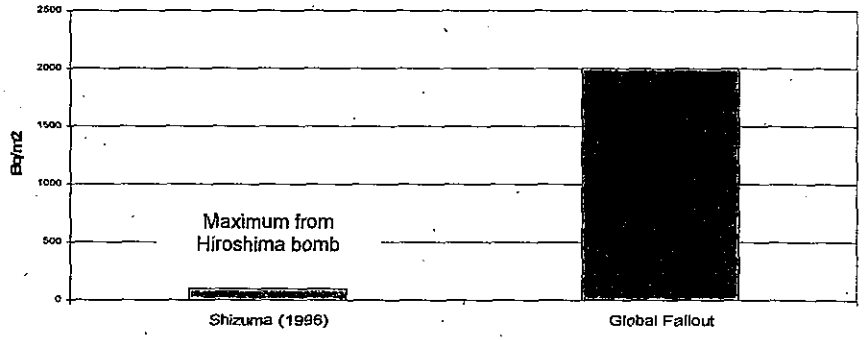

Fig. 1. Effects on global testing on ^{137}Cs

The following diagram (Fig. 2) shows that even at one latitude there is much variation in ^{137}Cs deposition. This is often due to differing rainfall. This diagram is due to (Aoyama and Hirose, 2003).

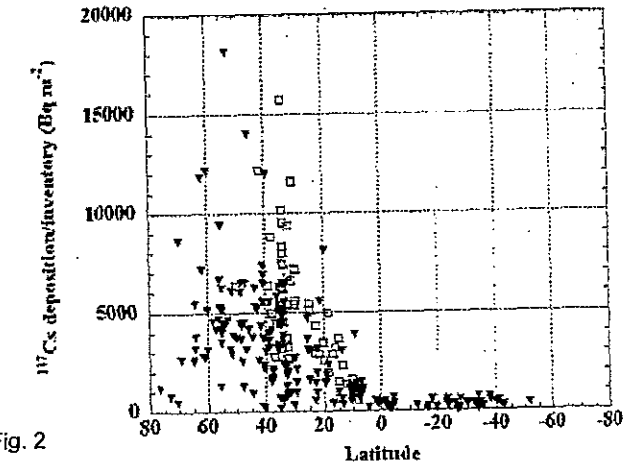

Fig. 2

Fig. 1 Meridional distribution of ^{137}Cs inventory at the stations in the North Pacific in the 1950s and decay corrected cumulative deposition at world-wide land stations as of end of 1965. Open square: ^{137}Cs inventory at the stations in the North Pacific in the 1960s Solid triangle: Decay corrected cumulative deposition of ^{137}Cs at land stations as of end of 1965.

There is more rain with greater height. A world-wide rule-of-thumb is that there is an increase of 100mm of rain a year with 100 m increase in height. Since fallout deposition depends heavily on rainfall, it should increase if we compare the amounts found, for example by (Hashizume et al. 1977) with the heights of the sample sites from a topographical map; we should find that there is an increase. This is shown in the following diagram (Fig. 3):

These points were taken from a southern traverse supposed to be relatively free from local fallout, because the bomb debris was blown away to the north-west. The diagram shows an increase with height,

Fig. 3 Hiroshima, E,ESE (>8km)

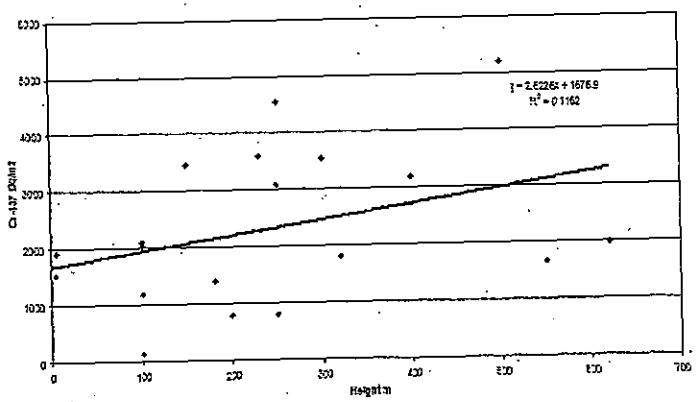

but only 12% of the relationship is explained that way – in other words, there is lots of scatter; the ^{137}Cs deposition is erratic. This is because the local rainfall does not depend just on height but on the local topography and may vary a lot in just a hundred meters horizontally, even at the same height.

Nevertheless an attempt was made to correct for the effect of height on ^{137}Cs deposition. From the above graph ^{137}Cs increases by about 300 $Bq.m^{-2}$ for each 100 m increase in height. When it is remembered the amount sought as local fallout (black rain) is about 100 $Bq.m^{-2}$, it is obvious that this may not succeed. However the estimated deposition at each sampling height was calculated and subtracted from the actual data and gave the following graph (Fig. 4).

Fig. 4 Hiroshima Cs-137 Predicted less Found

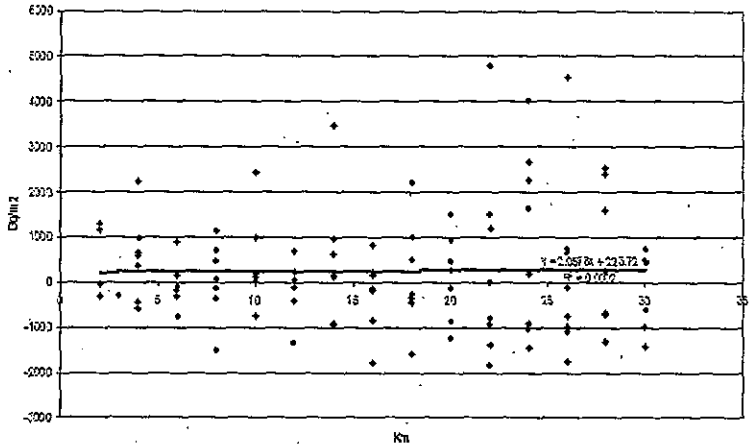

The above diagram shows that there is no significant trend with distance from the hypocenter, but an increase would have been expected, as ^{137}Cs is increasingly deposited. This means we cannot detect black rain by ^{137}Cs alone, at least using this method. However the approach adopted by Dr Cullings which examines the data by a different mathematical procedure to see whether nearby points are more like each other than would be expected has a better chance of detecting black rain.

The conclusion of this section is that the approaches above using ^{137}Cs alone, are not sensitive enough to detect black rain.

$^{239,240}Pu/^{137}Cs$.

It is commonly thought that ratios of fallout radionuclides should give more information. This is because in general they both are attached to particles and both precipitate in rain. The amount of rain is hardly important. This principle has already been applied to several Hiroshima soils from the Hashizume et al. survey by (Yamamoto et al. 1985). All values of the ratio were calculated as they would have been at the time of the Hashizume et al. survey in the last part of the '70s. The values were as follows (Fig. 5:"Density" means the number of observations for a particular X-axis Pu/Cs ratio):

Fig. 5 Histograms (Var1)

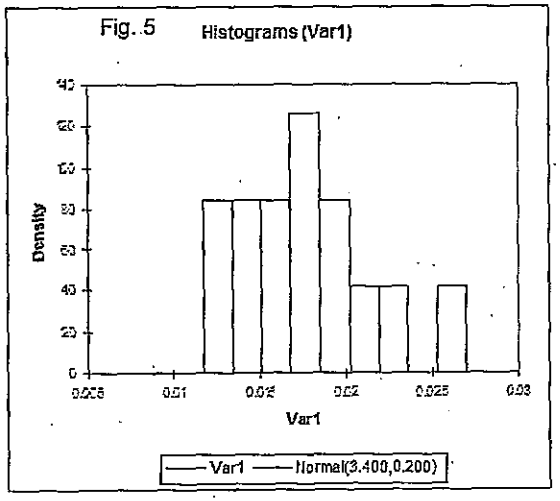

The median is about 0.015, and that was the global mean at that date. The authors concluded that there was probably no evidence of black rain, or local fallout.

The best set of similar soil data from that time is from the UK. (Cawse and Horrill, 1986; Cawse et al. 1988) They are as follows (Fig. 6):

Fig. 6 Histogram (Pu/Cs-UK)

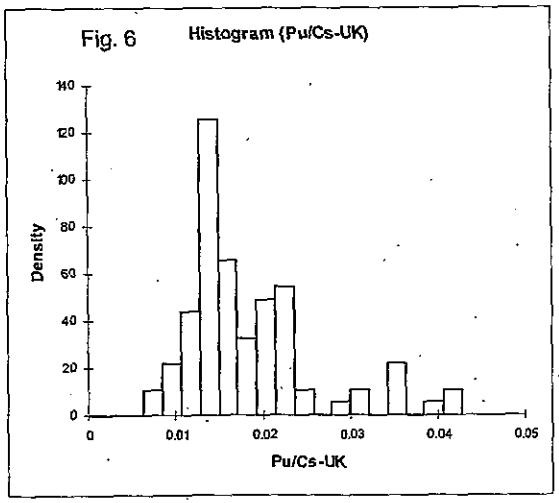

These data appear similar to the above Yamamoto et al. data.

However the number of samples in the above Yamamoto sample were limited, and subsequently our author from Kanazawa analysed many more of the soils from the survey for ^{137}Cs and $^{239,240}Pu$. We present the results shortly, but first calculate what Pu/Cs ratio would be expected at Hiroshima.

Using the detailed neutron fluxes between 10 keV and 1 MeV for the Hiroshima bomb published in (White et al. 2005), and $^{238}U(n,gamma)^{239}Pu$ cross-sections for the same energy range published in

(Panitkin and Tolstikov, 1972) which correspond well with previous estimates, the weighted mean cross-section which would correspond to this energy range is 128 millibarn.

We can calculate the estimated ^{239}Pu production and get $5.5*10^{10}$ Bq compared with 10^{14} Bq for ^{137}Cs, or a Pu/Cs ratio of 0.00055. This is much less than 0.015 for global fallout. But selective early Pu deposition as (e.g.) found between the Semipalatinsk testing ground and Dolon could increase this to 0.0055.

Black rain ought to have a distinctive signature: quite low Pu/Cs ratios. But the results from the data were as follows (Fig. 7):

Fig. 7 **Hiroshima and Global Background Pu/Cs**

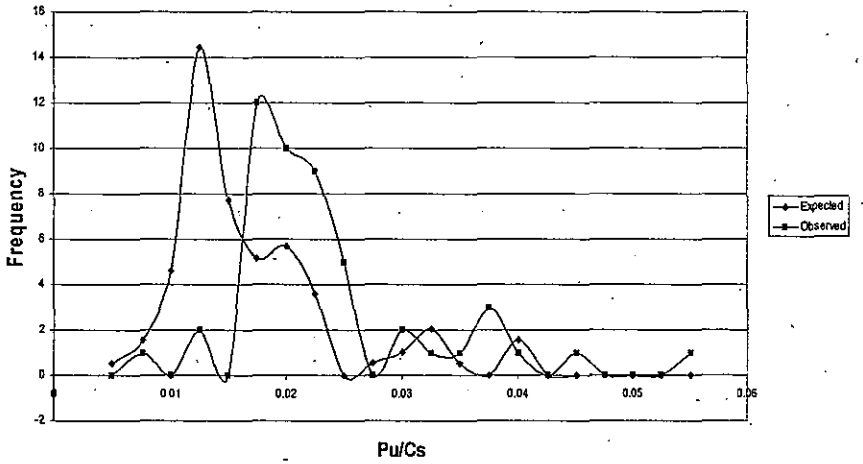

Fig. 8 **Comparison of ^{137}Cs-137, Yamamoto and Hashizume**

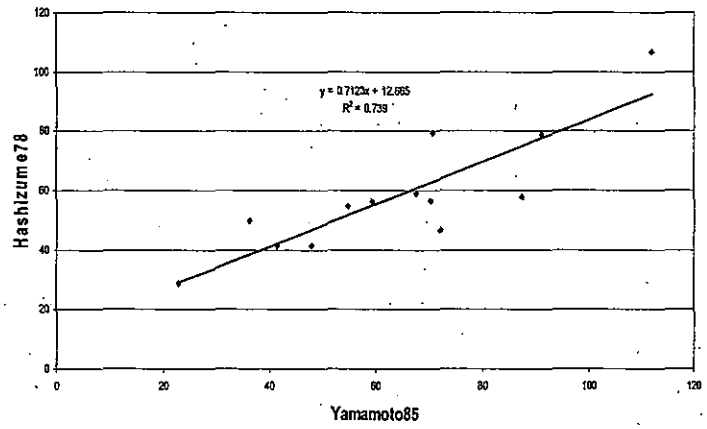

The above diagram is a kind of histogram, but presented as a graph, and the expected values are the background values from Cawse et al. The two curves are offset and it seems that the medians are not the same. It would seem that the observed values have a median of about 0.02 instead of 0.015. This is the opposite of what was expected - to detect black rain one would imagine obtaining Pu/Cs values lower than the global ratios.

The above diagram used the Hashizume et al. ^{137}Cs values. Our second author had analysed many of these same samples for ^{137}Cs. The next diagram (which eliminates one obvious outlier) compares the two analyses (Fig. 8). If there are no analytical problems, the points should all lie tightly clustered along a line with a slope of 1.00.

73.9% of the variance is explained which is reasonable, but the slope of the line is 0.71, not 1.00. This implies that there is a systematic error in the Hashizume data. Accordingly the Hashizume data are all divided by 0.71 and compared again against the background data (Fig. 9). This assumes that the Yamamoto Cs analyses are correct, but they have been tested internationally.

This shows that the two distributions are now almost coincident. They could be tested by a Chi-squared test to confirm this, but the numbers are rather small and the sensitivity would be not very great. A better test is a Normal Plot. This tests in a visual way whether more than one distribution is present. In the present case because the data look log-normal, a logarithmic transformation was used. The results of this plot for the Hiroshima data and the Cawse et al data looked complex, but generally the same except for three points with unusually low Pu/Cs ratios in the Hiroshima data which might have been local fallout.

Perhaps those lowest three points are black rain? These Pu values are fairly typical of global fallout, but the Cs values (7311, 5575 and 3304 Bq.m^{-2}) are high compared with the mean of about 2000 Bq.m^{-2} for Hiroshima. Since we expected a maximum of 100 Bq.m^{-2}, for black rain it is clear we are instead seeing global fallout, even for those three lowest points.

We expected a Pu/Cs ratio of 0.00055 and instead the lowest value is about 0.01. There is therefore no evidence by this method of local fallout, or black rain.

Fig. 9 **Hiroshima Corrected Pu/Cs Ratios**

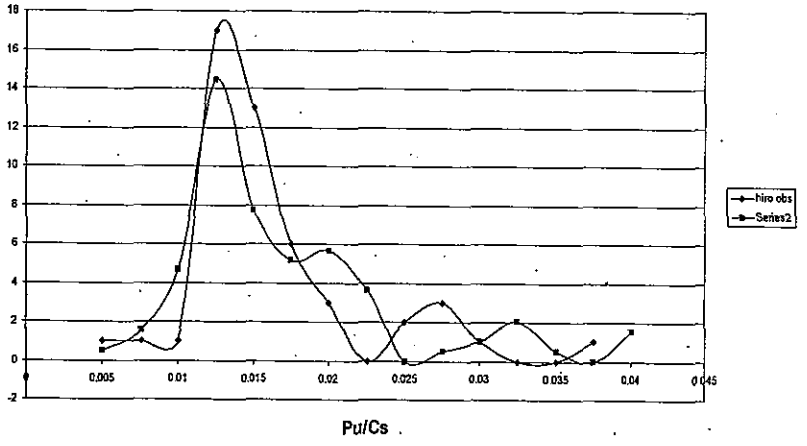

The entire data set for Hiroshima with other analyses is being prepared for publication. It may be that the best demonstration of black rain at Hiroshima remains the work of (Fujikawa et al. 2003) which found anomalous $^{235}U/^{238}U$ ratios. However the precision required is high and MC-ICPMS, TIMS or AMS would be needed. Some of this data is being produced by Sahoo et al. from NIRS at Chiba, and we believe is being reported elsewhere.

Some other characteristics of the carbon particles within black rain.

It was universally observed that the colour of the mushroom cloud was mostly white and other colours (including black) were minor. This arises from the chemistry of the cloud, which consisted of bomb particles, wood decomposition products including water vapour, and other debris from the ground.

First the many tonnes of the bomb material were volatilized and all chemical compounds decomposed, then rapidly as temperatures dropped most elements became oxide particles, chiefly ferrous oxide. Secondly and very rapidly, products from the decomposition of the buildings of Hiroshima were added.

Meteorologists from the Hiroshima Meteorological Bureau observed and sketched the mushroom cloud (sketches are in the Memorial Peace Museum) and recorded that black smoke was sucked up towards the fireball even in the first seconds and continued for hours afterwards.

The fireball which created temperatures on the ground of about 3-4000°C instantly created a mixture of black pyrolysed wood, (partial ashing, the black smoke) and further decomposition products of it. It is the partial ashing which gave the black particles visible in the black rain. Ashing of wood at higher temperatures of about 700°C gives a residue of white carbonates and silicates, chiefly of potassium and calcium, with some other more minor elements. Minute particles of silicon dioxide from the silicon content of wood would also be produced directly or indirectly. At the much higher temperatures of the bomb these will decompose, first to the elements, but as temperatures drop, to the oxides of the elements. Much of the organic matter is transformed to carbon dioxide and lost. It is only at temperatures much lower than 700°C, that unburnt carbon survives from the pyrolysis of wood to be carbon particles.

This carbon was therefore presumably mixed with radionuclides and could absorb them. The first black rain was recorded within about 15-20 minutes, and increased thereafter for several hours. It theoretically would contain absorbed radionuclides, and also less visible particles from the ashing of wood, which had also adsorbed radionuclides.

It should be noted that the black particles particularly were formed in a time range which extended much later than the bomb particle formation. This could easily lead to differences in radionuclides absorbed.

Particles of either bomb fragments or completely volatilized wood would be similar, in that both would be oxides, and ^{137}Cs and other volatile elements would not attach well. One figure frequently encountered in the literature is that perhaps 1.5% of ^{137}Cs would attach to such oxidic particles in general. Even less would attach of volatile elements as Iodine, Xenon and Tellurium. Other radionuclides are generally known to attach much more readily to such particles, particularly the rare earth elements. Eventually, but on a time scale of many days ^{137}Cs particularly, does attach to larger particles and precipitates with rain.

It should be noted that the volatilization of wood structures leads to another oxide – water - which when temperatures are low as in the upper atmosphere, will form rain. This did not happen in the desert

Trinity test in Nevada where negligible organic matter was volatilized. The appearance of some parts of the mushroom cloud at Hiroshima was thought by the observing meteorologists to be very like cumulus clouds and did contain much water, obviously enough to produce rain shortly thereafter.

The oxidic particles are mostly very soluble in water and if they predominate, any rain will be transparent, but may still have significant radionuclides attached. The fact that rain was not black is no guarantee of radiological safety.

Is the chemistry of the carbon particles any different from that of oxide particles? Does ^{137}Cs attach to black rain particles and precipitate as black rain? This brief survey will answer that indeed, even elements normally thought volatile attach to black rain particles in a way not seen for the higher temperature oxide particles. Black rain particles are a kind of sponge.

This is because burning most material of vegetable origin even under relatively uncontrolled conditions creates the substance called activated carbon, though controlled burning is necessary for good yields. By activated carbon is meant a very spongey structure caused by extreme volatilisation of volatiles within the solid. This substance has been well known for many years for its absorptive properties, (both in the gas and liquid phase) and this depends not on chemical bonds but on physical absorption. Almost all substances are absorbed regardless of chemical form. Thus non-volatiles will be absorbed, but so will the volatiles. In fact activated carbon is already well known for absorbing Iodine, rare inert gases, like Radon, Xenon and Krypton, (which usually do not react chemically with other compounds) and was used historically for removing ^{137}Cs and ^{131}I from reactor waste water streams, though now supplanted by more efficient extractants.

There are two possible consequences of the presence of carbon particles. The first is that their chemistry probably leads to absorption of different radionuclides from other oxide particles. The second is that their occurrence may not be the same in time as the other oxide particles from the bomb, and they may be exposed to a different composition of radionuclides in the atmosphere. This means that there could be a different kind of element fractionation at early and later stages of rain. One would expect early rain to contain relatively few volatiles, including ^{137}Cs. Thus there would be early preferential precipitation in rain of elements such as the rare earths, and other refractory elements. If this process is continued long enough, the radionuclides left in the air would be greatly depleted in refractory elements. This happens even with dry deposition and is well known in soil samples from traverses away from Semipalatinsk, for example, but will be even faster when rainout occurs. At the latest stages, it could be in the extreme case that ^{137}Cs and the inert gases are predominant in the air and after absorption within activated carbon are deposited as black rain. This is hypothetical, but reasonable.

From the foregoing material we expect that some carbon particles are carried into the upper atmosphere quite early, and absorb various elements, but that refractory elements are likely to be predominant in any rainout. In late stages of black rain, we expect the composition may be quite different and volatile elements may even predominate.

Although it is not known for certain it is therefore possible that the black rain visible particles could affect the rain composition expected from other studies which do not involve it. Detailed modeling might be needed if this was important.

This could be an explanation of the patterns noted by Imanaka if explanation proves to be needed. He finds in areas where there is excess ^{235}U in soils which is a marker of bomb influence, that calculated refractory/volatile ratios should be high, as measured by ^{235}U /^{137}Cs ratios, but they are found to be not

nearly as high as the 100/1.5 (about 60) expected. This suggests some influence already of carbon particles. For black rain found in streaks on walls he calculates that the $^{137}Cs/^{235}U$ ratio has a value of 1.9-16.3, in other words the volatile element ^{137}Cs predominates.

Without a lot more data it is impossible to be completely sure that the above scenario is the explanation for the results he found, but it is not unreasonable.

Conclusion

A conclusion would be that probably all rain experienced at Hiroshima regardless of colour had the potential to contain significant quantities of radionuclides. In calculation of dose, the refractory/volatile ratios calculated from the $^{235}U/^{238}U$ ratios in soils are likely to be most generally applicable.

Reference List

Aoyama, M. and Hirose, K. (2003) Temporal variation of 137Cs water column inventory in the North Pacific since the 1960's. *Journal of Environmental Radioactivity.* 69, 107-117.

Cawse, P.A., Cambray, R.S., Baker, S.J. and Burton, P.J. (1988) AERE-R-12535, London: Harwell.

Cawse, P.A. and Horrill, A.D. (1986) AERE-R-10155, London: Harwell.

Hashizume, T., Okajima, S., Kawamura, S., Takeshita, K., Tanaka, E., Tanaka, H., Nishimura, K., Maruyama, T., Yamada, H. and Yoshizawa, Y. (1977) 52pp Not cited. (Tokyo): Japan Public Health Association.

Panitkin, Y.G. and Tolstikov, V.A. (1972) Radiative capture of neutrons by U238 in the 1.2-4.0 MeV range. *Atomnaya Engergiya* 33, 782-283.

Shizuma, K., Iwatani, K., Hasai, H., Hoshi, M., Oka, T. and Okano, M. (1996) 137Cs concentration in soil samples from an early survey of Hiroshima atomic bomb and cumulative dose estimation from the fallout. *Health Physics* 71, 340-6.

White, S.W., Whalen, P.P. and Heath, A.R. (2005) Source term evaluations. In: Young, R.W. and Kerr, G.D., (Eds.) *Reassessment of the Atomic Bomb Radiation Dosimetry for Hiroshima and Nagasaki, Dosimetry System 2002*, 1 edn. pp. 62-138. Hiroshima, Japan: Radiation Effects Research Foundation]

Yamamoto, M., Komura, K., Sakanoue, M., Hoshi, M., Sawada, S. and Okajima, S. (1985) Pu isotopes, 241Am and 137Cs in soils from the atomic bombed areas in Hiroshima and Nagasaki. *Journal of Radiation Research* 26, 211-223.

A preliminary geospatial analysis of ^{137}Cs measured in soil cores from Hiroshima

Harry M. Cullings

Radiation Effects Research Foundation, Hiroshima and Nagasaki, Japan

Abstract

In the 1970s researchers collected a large number of soil samples at distances up to 30 km from the hypocenter of the Hiroshima A-bomb in various directions. Those samples were measured for several key, long-lived fallout radioisotopes including ^{137}Cs. The ^{137}Cs results are of particular interest in regard to evaluating the possible presence of local radioactive fallout from the Hiroshima bomb in places where soil samples were not taken in 1945 and area radiation survey measurements were not made in 1945. Unfortunately, various countries were testing nuclear bombs in the 1950s and 1960s, in above-ground tests that ejected large amounts of ^{137}Cs into the upper atmosphere, producing fallout around the world. The deposition of this "global fallout" at different locations a few km apart can be quite different due to factors that affect local rainfall and retention of Cs in the soil. Any fallout from the Hiroshima bomb that remained in the 1970s in particular parts of the sampled area would have to be of a certain size in order to create a pattern that would emerge from the noise of the variable global fallout. A key statistical problem is to establish the relationship between amounts of residual ^{137}Cs from the Hiroshima bomb and the statistical power to detect a related pattern in the context of the global fallout, using methods such as geospatial hotspotting. A first step to solving this is to characterize the spatial covariance structure of the measurement data. A simple variogram plots the squared difference between pairs of measured values versus the distance between them, using a scalar distance for an isotropic variogram. This shows some spatial structure, i.e., spatially closer pairs are more alike. We can standardize the variogram by converting the measurements to counts and dividing each squared difference by its expected value under the assumption that each count is a Poisson variate with mean equal to some average deposition of ^{137}Cs in mCi/km^2 across the entire Hiroshima area, times a "size" of the measurement. By "size" we mean a value in counts per mCi/km^2 that is proportional to the product of bulk sample mass, chemical recovery of Cs, counting efficiency, and counting time. The standardized variogram, under certain reasonable assumptions of stationarity in the spatial process being measured, confirms a variation in deposition at different locations that is much larger than the variation expected from the counting statistics. We explore the relationship between ^{137}Cs in mCi/km^2 and terrain elevation based on the idea that average annual rainfall and the corresponding deposition of global fallout ^{137}Cs from the atmospheric inventory are functions of elevation. As the data on ^{137}Cs in mCi/km^2 appear lognormally distributed, we investigate the application of a spatial scan statistic for normally distributed data to the logarithms of the data.

Introduction

In 1976 the Japan Public Health Association collected a large number of soil cores from the Hiroshima area as part of a program funded by the Ministry of Health, and measurements were made by researchers at Hiroshima University (Takeshita et al. 1976). Those cores were collected at approximately two kilometer intervals of radial distance from the hypocenter, along several traverses at fixed compass angles.

The angles, measured clockwise from due north, were approximately 0, 30, 60, 90, 120, 180, 270, and 330 degrees. The angles are concentrated in northerly through westerly directions because the area of black rain after the bombing, except at shorter distances within the main part of the city, was principally in those directions, and the direction of prevailing winds after the bombing at the level of the resulting cloud of radioactive debris from the fireball was to the northwest. The other directions were used for comparisons. Areas where samples could be collected in the southerly directions were limited by the areas covered by the Seto Inland Sea.

Among other radionuclides, the long-lived gamma emitter ^{137}Cs, a common radioisotope in radioactive fallout, was measured in the samples. In soil that was exposed to rainfall and essentially undisturbed between 1945 and 1976, any deposition that occurred as local radioactive fallout from the Hiroshima bomb should show up as an additive excess above the levels from global fallout that occurred during the period from approximately 1948, when atmospheric nuclear weapons testing began in the former Soviet Union, until 1976.

We began this work by looking for a way to compare areas of reported black rain from other areas. Conventional statistical tests did not find a difference between levels measured in the areas of black rain as reconstructed by Uda et al. (1953) or Masuda (1989) vs. other areas. We then turned to the use of geospatial hotspotting with a spatial scan statistic, which is a way of finding areas of high concentrations. Along the way, we made a number of basic statistical calculations and exploratory analyses of the data, which are reported here.

Methods

Map Work

The sample locations are recorded on 1:200,000 scale topographical maps of Hiroshima prefecture, which were supplied in the form of digital images of the maps associated with the report of Takeshita et al. (1976). In order to obtain accurate sample locations, we took the associated image rasters and located them in geographical coordinates, i.e., longitude and latitude in the Tokyo datum, using their markings of longitude and latitude. For this work we used geographical information system (GIS) software: ArcGIS (Earth Sciences Research Institute, 2009). This allowed direct comparison to digital maps and other features such as the DS02 estimate of the Hiroshima hypocenter. We used the tools in the GIS to obtain estimates of the geographical coordinates of sample locations marked on the 1:200,000 scale topographical map, which we then used to obtain estimates of elevation above sea level with digital topographic maps. For some calculations, we converted the geographical coordinates to simple Cartesian coordinates in km, with an origin at the DS02 estimate of the Hiroshima hypocenter (Cullings et al. 2005), by the approximations

$$x_i = (long_i - long_0)(111.111)\left[\cos\left(\frac{34.3\pi}{180}\right)\right], \quad y_i = (lat_i - lat_0)(111.111),$$ where $long_0$ and lat_0 are the coordinates of the DS02 estimate of the Hiroshima hypocenter in the Tokyo datum: 132.457307 degrees east longitude and 34.391349 degrees north latitude.

Reconstruction of Raw Sample Counts

Unfortunately, the data available from Takeshita et al. (1976) include count rates and estimated standard deviations of those rates based on counting statistics, but not actual counting times. To obtain estimates of raw counts that could be expected to have Poisson distributions, we estimated the original counting times as the count rates divided by the squares of their estimated standard deviations, under the assumption that

the background count in the spectral region of interest for ^{137}Cs (i.e., the 662 keV peak) was small, i.e., < 1/10 of the net count, for all samples. More details are given in Appendix I. We also calculated a "size" for each measurement in units of counts per mCi/km^2, by dividing the reconstructed count by the reported value of mCi/km^2.

Geospatial Hotspotting

For the purpose of geospatial hotspotting, we assumed that each measured location represents the average deposition of ^{137}Cs in a geographical area (geospatial cell) containing it that consists of a sector of radial width 2 km and angular width $\frac{\pi}{6}$ (i.e., 30°) in the polar grid used to set up the sample locations. We used the spatial scan statistic SaTScan™, available online at www.satscan.org to search for "hotspots" of ^{137}Cs that would have a probability < 0.05 of occurring under the null hypothesis assumed by SaTScan. The null hypotheses we used are described further under Results, for the specific settings that we used, but they essentially amount to assuming that measurements at different locations are independently statistically distributed with means consistent with a uniform areal deposition of ^{137}Cs across the geographical area under consideration. SaTScan is a well-tested package that considers potential hotspots on the basis of spatial proximity, i.e., the centroid of any geospatial cell can be the center of a hotspot, and for various radii, the collection of all cells within a given radius constitutes a zone considered as a possible hotspot (Kulldorff 1997). Because of its method of constructing candidate zones to be considered as possible hotspots, SaTScan is generally limited to finding circular hotspots, although it has an option for a certain range of elliptical hotspots. We did not use the settings for elliptical hotspots in this work, but the version we used has good properties for detecting elliptical hotspots even though the hotspot as shown by the software would have a circular shape (Kulldorff et al. 2006). Further details of the settings used are given below in Results.

Results

Map Work

Figure 1 shows the alignment of the 1:200,000 scale map that was done in the GIS using its markings of longitude and latitude. In this image, the 1:200,000 map is shown as a transparent overlay, i.e., a black line drawing of the map and an associated array of rays and concentric circles for marking sample locations at regular intervals in polar coordinates, which were part of the same image raster. One of the points used for alignment is the small, circular, magenta-colored marker near the bottom-left corner of the picture. It is aligned with the markings of longitude and latitude on the 1:200,000 scale map, which are the vertical and horizontal lines intersecting it. In the picture, the 1:200,000 map has been superimposed on portions of a new, 1:25,000 scale map dated April 1, 2002 (the colored blocks), to confirm its alignment using visible map features. Some features of the 1:200,000 scale map are not clear and well-defined even in the image raster shown here, which is the best available copy. Also, there are some areas along the seacoast on the newer map that are not shown in the older map, probably because they were reclaimed from the sea in the time between the production of the older and newer maps. However, it seems apparent that the older map is properly aligned, based on the outlines of major portions of the seacoast, islands etc.

When the image raster of the 1:200,000 scale map is geographically located in the GIS as described above, it appears that the hypocenter suggested by the origin of the sample grid of concentric circles and rays is misaligned with the DS02 estimate of the hypocenter: it is about 750 m from the DS02 estimate, almost due south. This relationship is shown near the top of Figure 1, in which the DS02 hypocenter is marked by a cross-shaped symbol, colored red to enhance its visibility.

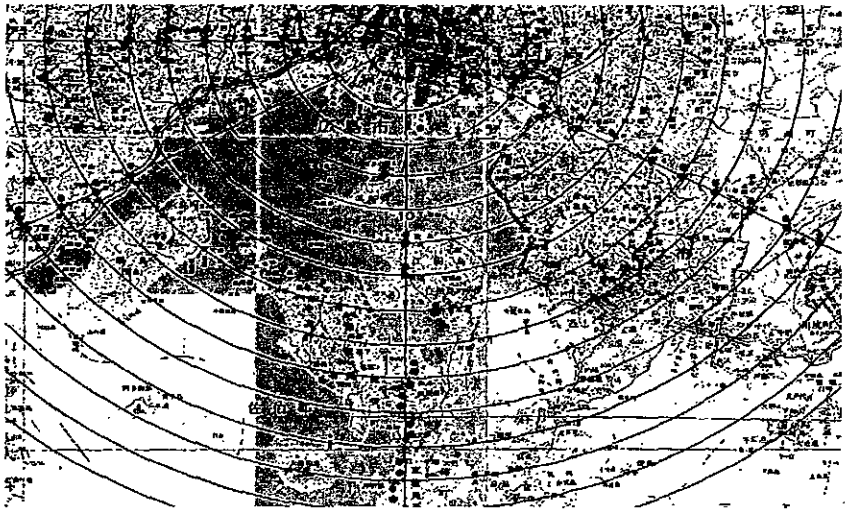

Figure 1. Alignment of sample map.

The implications of this misalignment for the sample locations depend on whether the sample locations in the image of the 1:200,000 scale map were determined by the sample grid, which is misaligned, or by the underlying features of the map itself. It appears more likely that the sample locations were determined by the sample grid, and are therefore about 700 m too far south. For example, there is a problem with the location of Sample No. 294, slightly less than 6 km south of the hypocenter, just east of due south, visible in the image of Figure 1 as the upper half of a black circle. (This location is more clearly seen in other images of the same map, not shown here.) The sample location as marked is about 700 m south of the southern tip of the small island associated with Ujina Port (Motoujinamachi). That location is inconsistent with the map features on the 1:200,000 scale map because it is in the sea, but is consistent with being drawn about 700 m too far south. We confirmed the misalignment by examining two of the 1976 sample locations, 12 and 14 km north of the hypocenter, that are depicted on much larger scale (about 1:10,000) maps associated with a later sample collection in 1978 (Hashizume et al.). It seems likely that the most correct estimates of the 1976 sample locations in geographical coordinates, except for those shown in the larger-scale maps from the 1978 work, are obtained by taking locations about 700 m north of those marked on the supplied image of the 1:200,000 scale map, i.e., the red circles in Figure 1. In the original paper map, at 1:200,000 scale, this 700 m shift represents only a 3.75 mm misalignment, which could easily have occurred in manual work with a paper map and something such as a transparent overlay of the sample location grid.

In the remainder of this work, we used sample locations based on geographical coordinates 700 m north from those marked on the map. That really only affects the elevations used for evaluating the relationship between measured values and elevation—because it is a uniform translation (all sample locations move by the same amount in the same direction), it does not affect the spatial variograms or the geospatial hotspotting described below. Unlike direct dosimetry with the A-bombs, the exact ground distance from the hypocenter to the measured locations is not critical in this work and is not as serious an issue in relation to the misalignment. For completeness, the map coordinates and the associated elevations that were obtained from digital topographic maps are shown in Table 1 for both sets of locations.

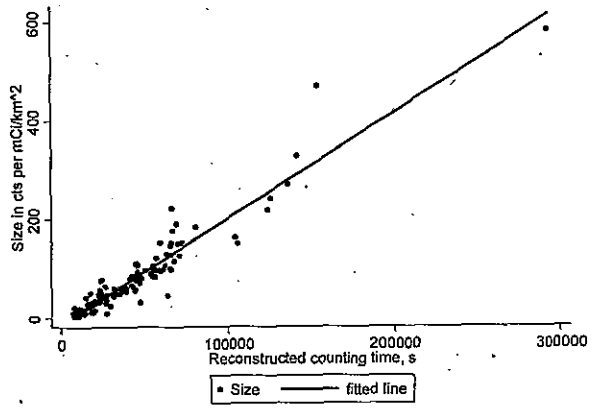

Figure 2. Linear relationship of sizes and counting times for the samples.

Reconstructed Counting Times and Sizes

The reconstructed counting times varied widely, with most samples being < 86,400 s (24 hrs) but about 8 samples having considerably larger counting times. A regression of "size" on counting time gave a strongly linear and plausible relationship, as illustrated in Figure 2, suggesting that the calculated "sizes" in counts per mCi/km^2 were primarily determined by counting times, as one might expect, and determined to a much lesser extent by variation in other factors, e.g., the mg amount of Cs recovered in each sample.

Distribution of Measured Values

Examination of the data revealed one extremely low value: Sample No. 529, 3.3 mCi/km^2. That sample has an unusually high estimated counting standard error of 0.059, i.e., a coefficient of variation = 0.174, whereas the coefficient of variation of the estimated counting error is less than 0.067 for all other samples and about 0.02 to 0.03 for almost all samples. When Sample No. 529 is omitted, the logarithms of the measured values are quite consistent with a normal distribution, based on standard statistical tests such as

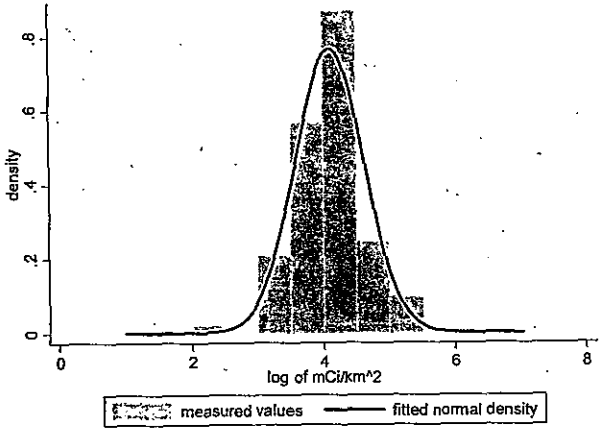

Figure 3. Distribution of logarithms of measured values.

those using estimates of skewness and kurtosis. A histogram of the logarithms of the measured values is compared to the normal distribution with the same mean (4.1) and standard deviation (0.52) in Figure 3. In most of the remaining work we omitted the result for Sample No. 529 and assumed the measured values to be distributed lognormal.

Classification by Rainfall Patterns

Using one of the supplied map images on which the rainfall patterns of Uda et al. (1953) and Masuda (1989) had been drawn, we classified the measurements as shown in Figures 4 and 5, with respect to the rainfall patterns. When we performed standard analysis of variance (ANOVA) procedures on the logarithms of the data, separately for the Uda and Masuda classifications by rainfall level, no statistically significant result was found. This is consistent with the relationships shown in the histograms in Figure 6.

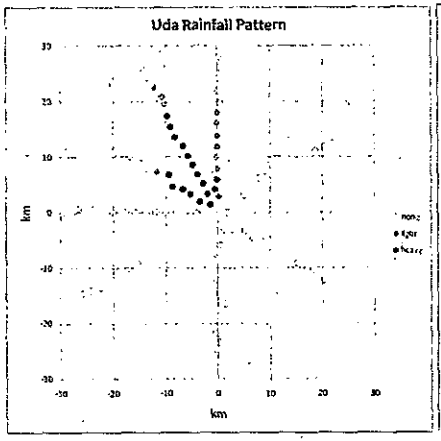

Figure 4. Soil core locations classified by the rainfall patterns of Uda.

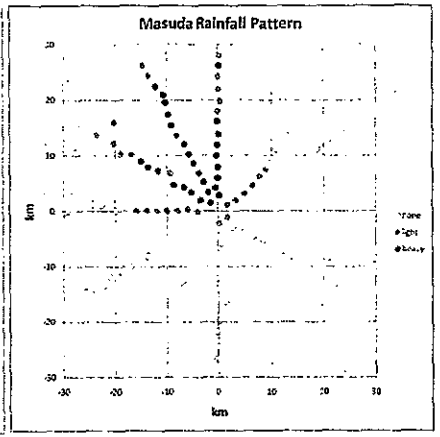

Figure 5. Soil core locations classified by the rainfall patterns of Masuda.

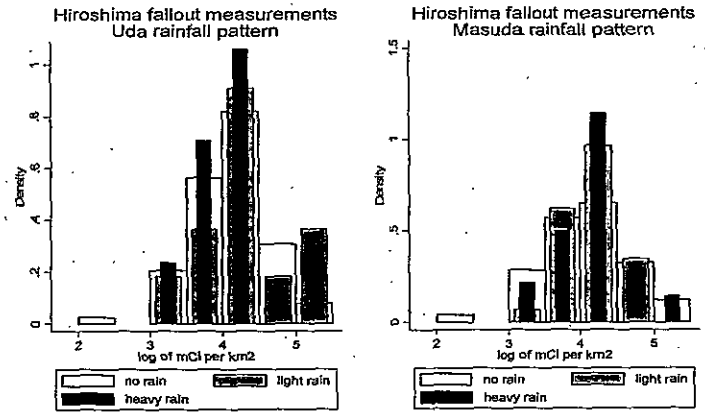

Figure 6. Histograms of logarithms of measured values classified by rainfall pattern.

Measured Amounts vs. Elevation

The measured values are plotted vs. elevation in Figure 7, using the elevations determined by the "700 m north" locations. The error bars are one standard deviation of the estimated counting uncertainty. The value measured by Shizuma et al. (1996) in a very early sample taken three days after the bombing, for the Koi-Takasu area of known fallout, corrected for radioactive decay to 1976, is shown as a red horizontal line for comparison. The very low measured value of Sample No. 529 is shown in this plot as well. When a simple linear regression (ordinary least-squares regression) of measured value on elevation is performed, a statistically significant slope estimate is obtained. The result is shown in Figure 7 as a trend line.

However, a linear regression of this type is inappropriate for lognormally distributed errors. Although one might consider a log-log regression, which would yield an estimated power function of measured value as a power of elevation, there are problems with this approach. One is that the data appear heteroscedastic: the dispersion increases with increasing elevation, as seen in Figure 8, in which we plot the logarithms of the measured values against the logarithms of the elevations. Another is that there are substantial errors in the elevations due to uncertainty in the exact sample locations. For those reasons, no attempt is made in the following calculations to adjust for elevation based on the linear regression.

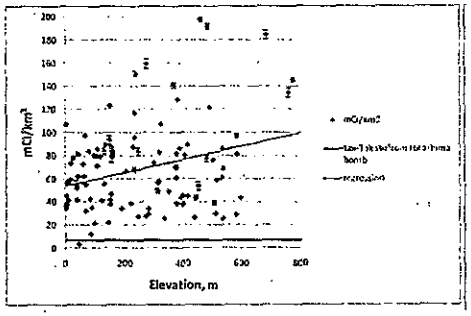

Figure 7. Measured values vs. elevation at sample location.

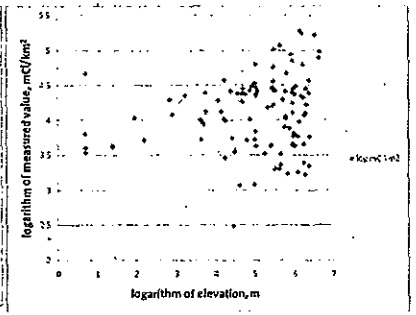

Figure 8. Logarithms of measured values vs. logarithms of elevations.

Spatial Patterns and Spatial Covariance Structure

The measured values are plotted in two dimensions in Figure 9, using a color scale running from dark blue (lowest values) through lighter blue, green, yellow, orange, light red to dark red (highest values), to illustrate the spatial patterns involved. To obtain an isotropic variogram (Cressie 1983) that is standardized with respect to the variance in measurements expected on the basis of the estimated counting uncertainty, we calculated $\frac{(A_i - A_j)^2}{\hat{\sigma}_i^2 + \hat{\sigma}_j^2}$ for all possible pairs of measured sample locations $\{(i,j)\}$, where $\hat{\sigma}_i$ is the estimated standard deviation of the uncertainty in the measured value A_i in mCi/km^2, based on the measurers' estimate of counting error. Then we divided the resulting values into 1,000 distance categories based on quantiles of the scalar distances d_{ij} between the locations in each pair, calculated the average of this quantity for each distance category, and used a lowess smooth with a bandwidth of 0.7 to produce the plot in Figure 10. There is considerable covariance among measured values at distances less than about 20

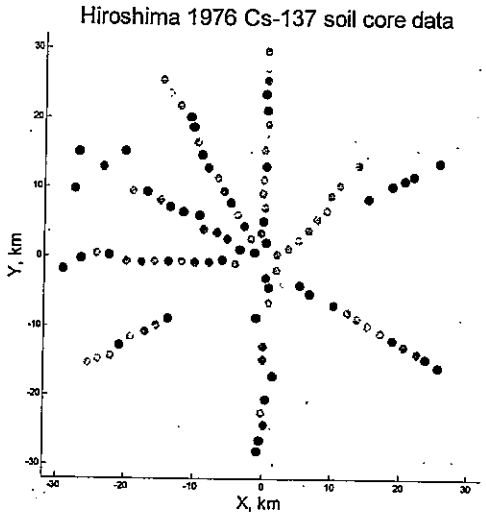

Figure 9. Plot of measured mCi/km^2 (marker color) vs. location.

km, as seen in the trend of the variogram at these distances. This is reflected in the patterns visible in Figure 9, where local areas of similar measured values are evident.

Moreover, the variogram is >>1 for all distances, consistent with the data's being much more disperse than the counting statistics would justify. This is also apparent in Figure 7, as the vertical dispersion of the plotted measured values is much larger than would be suggested by the error bars on the individual plotted values.

Geospatial Hotspotting

When we set out to use the spatial scan statistic SaTScan to look for hotspots, we first tried using the setting for Poisson distributed values, and applied it to the reconstructed raw gross counts. For that exercise, we calculated a "size" of each measured result, which SaTScan requires for Poisson data. We

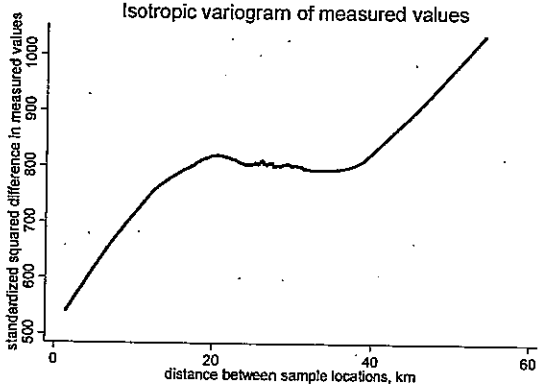

Figure 10. Standardized isotropic variogram of measured mCi/km^2.

specified "size" s_i in counts per mCi/km^2, calculated from the data by simply dividing the reconstructed raw count of a sample by its reported value in mCi/km^2. That calculation embodies the measurers' calculations that were based on the bulk sample mass, chemical and physical recovery of Cs, counting efficiency, and counting time for each sample. Then we multiplied this value times the weighted average value of mCi/km^2 for the entire set of samples, to obtain an expected value of the Poisson distributed count for each sample that is consistent with the null hypothesis of the spatial scan statistic, that the true value of mCi/km^2, say $\tilde{A}$, is constant over the geographical area of the measurements, and the variation among measurements is due to the variation in independently distributed Poisson random variables A_i, one at each measured location, with expected value $E\{A_i\} = \mu_i = s_i \tilde{A}$.

The Poisson application of SaTScan yielded many apparent hotspots, > 10, many of which consisted of individual measured locations, and those putative hotspots were distributed throughout the area covered by the sample grid. The result is consistent with the gross over-dispersion relative to the Poisson distribution that is noted above, but it is not very useful.

A more realistic application of SaTScan is obtained by noting that the data appear to be lognormally distributed overall. As SaTScan has a setting for normally distributed data, we can use this with the logarithms of the measured values. Unfortunately, there is no straightforward way to use SaTScan for a compound model in which we would assume as a null hypothesis that the true value at each sample location is a sample from a lognormal distribution but is measured with uncertainty that depends on the measurement "size" through Poisson counting statistics and the "size" of the sample/measurement. For example, attempting to adjust the analysis for the varying precision of the measurements by setting the "number of cases" equal to the "sizes" of the samples in mCi/km^2 is not correct because SaTScan uses a permutation routine in Monte Carlo trials to determine the distribution of its likelihood ratio test statistic under the null hypothesis for the normal model (SaTScan™ User Guide, available at www.satscan.org). The permutation method used by SaTScan does not preserve the covariance structure of a "lognormal plus Poisson" null hypothesis.

However, we can assume that all measurements are effectively measured with equal uncertainty, by setting the "number of cases" = 1 for all measurements in the SaTScan input file, and we can apply SaTScan, with a setting for normally distributed data, to the logarithms of the measured values. That is, in doing so we assume as a null hypothesis that the measured values are independently and identically distributed ("iid") lognormal, with parameters that SaTScan implicitly estimates by permuting measured values among geospatial locations to form the distribution of its likelihood ratio test statistic in Monte Carlo replications under the null hypothesis. This is not strictly true, because we believe that there is an effect of terrain elevation, and for that reason among others we might expect some spatial covariance structure that violates the assumption of independence. However, spatial scan statistics have generally not been developed for null hypotheses involving known spatial covariance structures, and the "iid" assumption may still be a useful null hypothesis for geospatial hotspotting in the present work. We just need to be aware that any apparent hotspots might be due to effects of elevation or other factors with local spatial structure, on the deposition or retention of global fallout. It seems reasonable to ignore the variable precision of the measurements in this analysis, in light of the fact that the estimated measurement uncertainty has a coefficient of variation on the order of 0.02 to 0.03, maximum 0.066, as noted above, which is much smaller than the coefficient of variation of the measured values among locations, which is

0.55. The result is that SaTScan does not find any statistically significant hotspots. The output from SaTScan is given in detail in Appendix II.

Discussion

It seems reasonable that the spatial covariance structure in the data is due primarily, if not completely, to factors such as terrain elevation and slope, soil type, and other factors that have similar spatial structure and affect the deposition of global fallout and the retention after weathering of all fallout including that from the Hiroshima bomb. The lognormal distribution of the data, which is a common observation in environmental samples, is presumably due to a combination of multiplicative factors that affect the final measured results. Some of these factors may be associated with the original deposition of ^{137}Cs from global fallout, which varies from place to place, but many of them are undoubtedly associated with local variations in the retention of all deposited ^{137}Cs, both that from the Hiroshima bomb and that from global fallout, under the process of weathering.

It is unfortunate that we cannot make a simple adjustment for elevation that would presumably capture the effect of elevation on deposition of global fallout via its effect on long-term average rainfall. Unfortunately, however, it seems clear that this effect of elevation, even if we are certain it had a linear effect on deposition, preceded a large part of the variation that produced the lognormal distribution of the data, and therefore is multiplied by a succession of multiplicative factors that in the aggregate impart a lognormal variation. Accordingly, if a simple adjustment based on the slope of the linear regression of mCi/km^2 on elevation is made to the data, they no longer appear lognormal in overall distribution. More specifically, the simple linear regression is not correct for a number of reasons:

- The overall distribution of the data among sample locations is lognormal, not normal, and it is reasonable to assume that the dispersion about the mean function in the regression should be a combination of
    - a lognormal variation in the true values of mCi/km^2 at sample locations of equal elevation and
    - a much smaller measurement error that is dominated by Poisson counting statistics;
- A simple linear regression is not correct for lognormal errors;
- The errors are heteroscedastic, as described above, i.e., they increase with increasing elevation and the corresponding size of the mean function in the regression, which requires some form of weighting or estimation of a variance function in the regression; and
- There is non-negligible error in the estimates of site elevations (the independent variable in the regression), which creates an "errors in variables" problem in the regression (Carroll et al. 2006).

Therefore, it does not appear to be possible to make corrections for elevation without 1) a specific and rather complicated stochastic model for local area specific deposition and weathering and 2) a sophisticated method for a regression or other estimation procedure to relate elevation to the eventual measured values. This does not appear feasible at present.

Unfortunately, it is not possible to directly compare the 1976 measurements to measurements of 1945 samples in the known fallout area of Koi-Takasu. The closest to Koi-Takasu of the 1976 samples is 4 km due west of the hypocenter. This is about 2.1 km northwest of the location of sample No. 7 of Shizuma et al. (1996), which was much hotter than their other samples and is the sample on which the horizontal line in Figure 7 of this work is based. The location of sample No. 7 of Shizuma et al. (1996) was part of an area extensively reconstructed after the typhoons of 1945, with rerouting of the rivers (Yamate-gawa and Fukushima-gawa), and it may have been impossible to find undisturbed soil for sampling in 1976 in the generally acknowledged fallout area of Koi-Takasu.

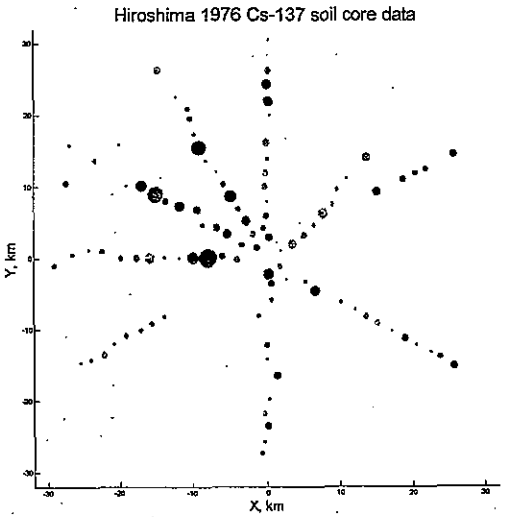

Figure 11. Measurement size. Key: marker size = measurement size marker color = mCi/km^2

Because the application of SaTScan for normal data to the logarithms of the measured values does not produce a significant hotspot, it would be of interest to know how large an original deposition of ^{137}Cs from the Hiroshima hotspot would have a given probability of being detected by this method. Although it is generally accepted that a deposition similar to the known local fallout area at Koi-Takasu would not be detectable in the context of accumulated global fallout (Shizuma at al. 1996), and that appears to be correct, even if spatial methods are used, larger amounts presumably would be detectable. Future work may focus on using alternative models of deposition and weathering/retention to make such calculations by Monte Carlo simulation, akin to a statistical power calculation. Because of the asymmetrical geospatial distribution of the measured locations, simulations must make fairly specific assumptions about the locations of areas of deposition in relation to sampled locations, at least for the original deposition from the Hiroshima bomb. They could be performed for complementary models that assign all of the lognormal variation to deposition vs. models that assign all of it to weathering. They could also include an effect of elevation on deposition of global fallout. It may also be possible to use a hierarchical model to add some form of spatial covariance to the simulations, similar to what is reported here and described in the variogram.

There is another problem with evaluating the power of the geospatial hotspotting to detect an effect of some specified size and pattern, which relates to the way in which the sample "sizes" were determined by choice of counting times, which is not random. The sample sizes are shown in Figure 11, in which the size of each marker is proportional to the size of the sample and the color of the marker is related to the measured result in mCi/km^2 as in Figure 9. As shown in the figure, almost all of the really large sample sizes are in westerly to northerly directions, and involve relatively low measured values. It is logical to surmise that those came about because the measurers extended the measuring times of some of the samples, mainly those initially yielding low results in areas where higher results were expected. Correcting for that intervention in a post hoc analysis, especially without detailed knowledge of how the decisions about counting times were made, is a very difficult statistical problem. It may still be necessary

to rely on the assumption, as noted above, that the variation in counting precision can be neglected because the counting uncertainty is small compared to the assumed variation of the true values of mCi/km^2 among sample locations.

Conclusions

Under reasonable statistical assumptions for a null hypothesis (i.e., that the measured values are independent samples (single values) drawn from a single lognormal distribution, due to effectively random variation in deposition and retention of global fallout at each sampled location, with a variance much larger than the variances of the measurements due to counting statistics), the spatial scan statistic found no significant hotspots. An interesting question that remains to be answered is, if we assume as an alternative hypothesis 1) a specific amount of deposition in 1945 from the Hiroshima bomb in specific areas associated with the black rain, 2) a later deposition of global fallout that has a certain spatial variation from place to place in the sampled area, and 3) a model for removal of both of these by weathering; how big would the deposition from the Hiroshima bomb have to be, in order to have a given probability of being detected with the spatial scan statistic under the null hypothesis described above? That question can be answered under certain restrictive but reasonable assumptions with a future simulation study.

Acknowledgements

The Radiation Effects Research Foundation (RERF), Hiroshima and Nagasaki, Japan is a private, non-profit foundation funded by the Japanese Ministry of Health, Labour and Welfare (MHLW) and the U.S. Department of Energy (DOE), the latter in part through the National Academy of Sciences. This publication was supported by RERF Research Protocol RP #18-59. SaTScan™ is a trademark of Martin Kulldorff. The SaTScan™ software was developed under the joint auspices of Martin Kulldorff, the National Cancer Institute, and Farzad Mostashari at the New York City Department of Mental Health and Hygiene.

References

Carroll RJ, Ruppert D, Stefanski LA, Crainiceanu CM. *Measurement error in nonlinear models: a modern perspective* (2nd ed.). Chapman & Hall, Boca Raton, Florida, USA (2006).

Cressie NAC *Statistics for spatial data* (revised edn). John Wiley & Sons, New York, NY (1993).

Cullings HM, Fujita S, Hoshi M, Egbert SD, Kerr GD Alignment and referencing of maps and aerial photographs. In: Young RW, Kerr GD (eds) Reassessment of the atomic bomb radiation dosimetry for Hiroshima and Nagasaki – Dosimetry System 2002. Radiation Effects Research Foundation, Hiroshima, Japan, pp 139-222 (2005). http://www.rerf.jp/shared/ds02/index.html Accessed 28 March 2010

Hashizume T, Okajima S, Kawamura S, Takeshita K, Tanaka E, Nishimura K, Tanaka H, Maruyama T, Yamada H, Yoshizawa T. Study on residual radioactivity in Hiroshima and Nagasaki. J Hiroshima Med Ass 31: 455-458 (1978).

Kulldorff M A spatial scan statistic. Commun Stat Theory Methods 26:1381-1496 (1997).

Kulldorff M, Huang L, Pickle L, Duczmal L An elliptic spatial scan statistic. Stat in Med 25:3929-3943 (2006).

Masuda, Y. Re-investigation about "black rain" after Hiroshima A-bomb. *Tenki* 36: 69-79 (1989).

Shizuma K, Iwatani K, Hasai H, Hoshi M, Oka T, Okano M. ^{137}Cs in soil samples from an early survey of Hiroshima atomic bomb and cumulative dose estimation from the fallout. Health Phys 71(3): 340-346 (1996).

Takeshita K, Sunayashiki T, Takeoka S, Kato K. ^{137}Cs in soil of the black rain area northwest of the Hiroshima hypocenter. Hiroshima: pages 109-115. Research Institute for Nuclear Medicine and Biology, Hiroshima University, Hiroshima, Japan (1976).

Uda M, Sugahara Y, Kita I. Meteorological conditions related to the atomic bomb explosion in Hiroshima. In: Collection of reports on investigations of the atomic bomb casualties, pages 98-136. Science Council of Japan, Tokyo (1953).

Appendix I: Reconstruction of Raw Counts for the Hiroshima University Data on ^{137}Cs Measured from Soil Cores

Assumptions and notation:

- t is the counting time in seconds.
- N_P is the total count in m_P channels selected as the region of interest (ROI) for the 662 keV peak.
- N_B is the total count in m_B neighboring channels used to determine background.
- The sample net count is calculated as $N_{net} = N_P - N_B \frac{m_P}{m_B}$ and the sample net count rate cps is calculated as $cps = \frac{N_{net}}{t}$.
- N_B is distributed Poisson(μ_B), where μ_B is the same for all samples (assuming no significant artifacts due to interfering signal in the areas selected for background, which should be true, and no significant changes in signal gain or other causes of a change in μ_B from count to count).
- N_P is distributed Poisson($\mu_B + \mu_P$), where μ_P is the true mean net count rate in the peak ROI for the sample being measured.
- SD is calculated as $SD = \frac{\sqrt{N_P + \frac{m_P}{m_B} N_B}}{t}$.

This results in the relationship $\frac{cps}{SD^2} = t \frac{N_P - \frac{m_P}{m_B} N_B}{N_P + \frac{m_P}{m_B} N_B}$.

- For very low net count rates, $\frac{cps}{SD^2} \to 0 \quad as \quad N_P \to \frac{m_P}{m_B} N_B$, i.e., as the sample net count rate approaches background for a proper blank containing no ^{137}Cs.
- At high net count rates, for $N_P >> \frac{m_P}{m_B} N_B$, $\frac{cps}{SD^2} \to t$.

Appendix II SaTScan Results for the Assumption of Lognormally Distributed Values

SaTScan v7.0.3

Program run on: Fri Apr 09 14:52:22 2010

Purely Spatial analysis
scanning for clusters with high values
using the Normal model.

SUMMARY OF DATA

Study period.....: 1976/1/1 - 1976/12/31
Number of locations.....: 106
Total number of cases....: 106
Mean.....: 68.97
Variance.....: 1378.00
Standard deviation.....: 37.12

MOST LIKELY CLUSTER
1.Location IDs included.: 429, 424, 494, 419, 289, 414, 444, 449
Coordinates / radius..: (-27.5827,9.81943) / 10.02
Number of cases.....: 8
Mean inside.....: 116.00
Mean outside.....: 65.13
Unexplained variance..: 1195.75
Standard deviation....: 34.58
Log likelihood ratio..: 7.518513
Monte Carlo rank.....: 302/1000
P-value.....: 0.302

SECONDARY CLUSTERS
2.Location IDs included.: 264, 209, 269, 204, 504, 259, 509, 254, 514, 219, 454
Coordinates / radius..: (0.164747,21.2153) / 10.83
Number of cases.....: 11
Mean inside.....: 94.63
Mean outside.....: 66.00
Unexplained variance..: 1301.07
Standard deviation....: 36.07
Log likelihood ratio..: 3.044578
Monte Carlo rank.....: 990/1000
P-value.....: 0.990

Table 1. Locations, elevations and mCi/km^2 of ^{137}Cs measured in samples.

		As marked			Shifted 700 m north			
Sample No.	mCi/ km2	longitude	latitude	elev., m	longitude	latitude	elev., m	diff. in elev., m
234	38.2	132.459104	34.411089	3	132.459104	34.417389	4	1
239	59.1	132.451157	34.422679	27	132.451157	34.428979	18	-9
194	41.2	132.455462	34.438573	18	132.455462	34.444873	121	103
199	78.8	132.45778	34.456124	150	132.45778	34.462424	155	5
214	79.6	132.454468	34.474667	39	132.454468	34.480967	116	77
219	82.6	132.455462	34.492218	408	132.455462	34.498518	319	-89
254	150.7	132.458111	34.509437	261	132.458111	34.515737	237	-24
259	66.2	132.456124	34.53063	420	132.456124	34.53693	203	-217
204	116.9	132.456786	34.547187	168	132.456786	34.553487	233	65
209	67.9	132.461422	34.563743	218	132.461422	34.570043	231	13
264	33.7	132.459104	34.582287	180	132.459104	34.588587	281	101
269	38.9	132.45778	34.603149	370	132.45778	34.609449	378	8
504	60.9	132.459436	34.620699	378	132.459436	34.626999	379	1
509	128.5	132.459104	34.637256	411	132.459104	34.643556	384	-27
514	97	132.459767	34.65878	754	132.459767	34.66508	585	-169
134	81.1	132.477539	34.394902	3	132.477539	34.401202	42	39
15	72.7	132.494856	34.402239	39	132.494856	34.408539	58	19
17	83.5	132.511879	34.413099	17	132.511879	34.419399	80	63
14	89.1	132.527435	34.426013	168	132.527435	34.432313	137	-31
19	79.6	132.541523	34.440982	161	132.541523	34.447282	106	-55
24	86.9	132.555611	34.452428	98	132.555611	34.458728	155	57
84	80.3	132.562949	34.471506	36	132.562949	34.477806	96	60
139	83.7	132.577037	34.485301	155	132.577037	34.491601	130	-25
499	43.7	132.622823	34.468278	331	132.622823	34.474578	393	62
149	81.9	132.607561	34.511423	149	132.607561	34.517723	378	229
524	27.3	132.660392	34.484127	307	132.660392	34.490427	246	-61
529	27.2	132.68035	34.491758	253	132.68035	34.498058	272	19
534	26.1	132.695319	34.497041	403	132.695319	34.503341	440	37
539	0	132.712342	34.515825	412	132.712342	34.522125	418	6
544	38.3	132.736703	34.515238	434	132.736703	34.521538	379	-55
60	77.9	132.476072	34.374943	2	132.476072	34.381243	25	23
244	106.6	132.486638	34.358214	2	132.486638	34.364514	2	0
65	41.4	132.513934	34.355572	3	132.513934	34.361872	38	35
249	36.7	132.529783	34.344126	17	132.529783	34.350426	2	-15
70	122.8	132.550622	34.338255	245	132.550622	34.344555	151	-94
75	49	132.567938	34.329744	257	132.567938	34.336044	351	94
89	83.4	132.590538	34.320645	252	132.590538	34.326945	246	-6
94	86.3	132.606094	34.31184	349	132.606094	34.31814	390	41
99	95.7	132.62341	34.303035	197	132.62341	34.309335	234	37
104	93.3	132.643075	34.293643	165	132.643075	34.299943	149	-16
109	45.2	132.662153	34.284544	577	132.662153	34.290844	397	-180
114	140.7	132.68035	34.275739	504	132.68035	34.282039	370	-134
119	53.6	132.702363	34.267228	504	132.702363	34.273528	453	-51
124	21.8	132.715864	34.260771	158	132.715864	34.267071	145	-13
129	37.8	132.736409	34.249324	137	132.736409	34.255624	151	14
574	44.9	132.459342	34.364964	0	132.459342	34.371264	2	2
339	34.3	132.463745	34.352931	3	132.463745	34.359231	2	-1
294	73.1	132.463745	34.332385	13	132.463745	34.338685	17	4
344	12.1	132.44496	34.312721	100	132.44496	34.319021	84	-16
299	56.6	132.45582	34.275739	36	132.45582	34.282039	7	-29
304	54.8	132.45582	34.258423	7	132.45582	34.264723	37	30
309	41.3	132.471963	34.237584	2	132.471963	34.243884	9	7
314	21.5	132.460516	34.207353	97	132.460516	34.213653	99	2

		As marked			Shifted 700 m north			
Sample No.	mCi/km2	longitude	latitude	elev., m	longitude	latitude	elev., m	diff. in elev., m
319	97.2	132.453765	34.189449	121	132.453765	34.195749	67	-54
324	51.7	132.458168	34.174187	3	132.458168	34.180487	40	37
329	3.3	132.452004	34.153935	19	132.452004	34.160235	44	25
334	31.9	132.448776	34.139554	45	132.448776	34.145854	68	23
349	42.6	132.306133	34.312134	7	132.306133	34.318434	83	76
354	62.1	132.287349	34.303035	19	132.287349	34.309335	62	43
359	55.5	132.269152	34.294523	66	132.269152	34.300823	131	65
364	87.3	132.247139	34.28836	384	132.247139	34.29466	229	-155
369	159.2	132.228648	34.2775	423	132.228648	34.2838	277	-146
474	79.9	132.213973	34.263706	278	132.213973	34.270006	405	127
479	76.1	132.194015	34.258423	499	132.194015	34.264723	502	3
484	77.7	132.177872	34.253726	479	132.177872	34.260026	479	0
30	62	132.412968	34.383455	2	132.412968	34.389755	42	40
35	34.1	132.390956	34.387858	200	132.390956	34.394158	189	-11
224	52.9	132.370117	34.385216	39	132.370117	34.391516	39	0
229	55.5	132.347811	34.385216	66	132.347811	34.391516	66	0
374	70	132.327559	34.38551	377	132.327559	34.39181	377	0
379	43.3	132.305546	34.385803	443	132.305546	34.392103	443	0
384	81	132.283827	34.38551	585	132.283827	34.39181	585	0
389	58.9	132.263575	34.385216	516	132.263575	34.391516	516	0
434	89.3	132.240095	34.38551	407	132.240095	34.39181	417	10
439	25.3	132.210744	34.394021	584	132.210744	34.400321	536	-48
444	134.2	132.190786	34.396076	670	132.190786	34.402376	760	90
449	191.5	132.166425	34.389912	47	132.166425	34.396212	486	439
489	44.6	132.138249	34.376117	482	132.138249	34.382417	415	-67
40	34.9	132.419425	34.401946	79	132.419425	34.408246	88	9
45	54.8	132.39888	34.415153	154	132.39888	34.421453	69	-85
50	46.8	132.382738	34.423372	76	132.382738	34.429672	152	76
55	57.8	132.361312	34.427187	167	132.361312	34.433487	318	151
154	25.6	132.354561	34.445971	355	132.354561	34.452271	338	-17
159	38	132.329613	34.450374	378	132.329613	34.456674	400	22
274	28.7	132.308481	34.456537	693	132.308481	34.462837	583	-110
279	60.8	132.292925	34.465343	559	132.292925	34.471643	533	-26
284	38.4	132.271793	34.475909	373	132.271793	34.482209	219	-154
289	68.6	132.249193	34.476789	486	132.249193	34.483089	538	52
419	121.6	132.235399	34.494106	488	132.235399	34.500406	492	4
414	39	132.236902	34.528462	512	132.236902	34.534762	506	-6
424	145.5	132.200472	34.508194	788	132.200472	34.514494	775	-13
429	43.3	132.156446	34.479724	653	132.156446	34.486024	598	-55
494	184.3	132.161729	34.527565	822	132.161729	34.533865	681	-141
174	37.4	132.442025	34.39813	3	132.442025	34.40443	4	1
164	73.7	132.436155	34.415447	205	132.436155	34.421747	300	95
169	56.7	132.425589	34.43159	419	132.425589	34.43789	316	-103
179	85.8	132.415316	34.446558	109	132.415316	34.452858	110	1
184	41.5	132.404163	34.462701	159	132.404163	34.469001	149	-10
189	56.4	132.393597	34.477376	221	132.393597	34.483676	318	97
394	81	132.383325	34.493519	232	132.383325	34.499819	156	-76
399	49.7	132.367475	34.507314	540	132.367475	34.513614	312	-228
404	29.9	132.357496	34.524043	423	132.357496	34.530343	512	89
409	71.2	132.350746	34.541066	223	132.350746	34.547366	107	-116
454	197.6	132.343995	34.560438	370	132.343995	34.566738	461	91
459	28.9	132.339886	34.572471	364	132.339886	34.578771	281	-83
464	84	132.32433	34.58744	162	132.32433	34.59374	159	-3
469	107.1	132.308775	34.604463	248	132.308775	34.610763	325	77
519	86	132.296154	34.620899	544	132.296154	34.627199	536	-8

おわりに

自分の原稿でも述べたように、京都大学原子炉実験所で開催した DS02 研究会の報告書をまとめながら、“黒い雨”放射能についていま一度キチンと問題を詰めておきたいと５年ほど前に考えはじめた。まずは、原爆直後の日米の研究者による放射能調査について、古い資料の検討をはじめた。一方、広島の星さんたちも同じような問題意識をもっていたようで、彼らが放医研のサフーさんに測定を依頼していた、黒い雨地域のウラン 236 のデータを見せてもらう機会があった。サフーさんのデータについて遠藤さん（当時広大原医研）らと discussion を深めながら、『ウラン 236 データが広島黒い雨放射能問題の break through になりそうだ』と思いはじめたところに、広島市役所の方から『黒い雨放射能の実態解明に関する検討会』をやりたいので協力してほしいという話が入ってきた。サイエンスの側と行政の側では『土俵とルール』が違っているので、行政と組むのには躊躇するところはあったが、行政と一緒の方がものごとを進め易いことも確かなので、市役所お膳立てではじめての検討会を開いたのが 2008 年２月だった。

広島市側としては、検討会の結論をもって黒い雨地域の被爆者援護策拡充のために役立てたい、という思惑がある。市の立場は理解できるし、我々の仕事の成果がその役に立つのは望むところでもある。しかしながら、行政の土俵で相撲をはじめてしまうと、意識的にしろ無意識的にしろ、どこかで自由度に制限を受けることになる。個人的には、『研究者の趣味としてやっているんであって、市に頼まれてやっているんじゃない』というスタンスで関わっていたが、足場がないと何かとやりにくい。そこで、みなさんにお願いして研究者の側として『広島“黒い雨”放射能研究会』という形を作らせてもらった次第であった。

本報告書は、市役所主催での４回の検討会、広大原医研で行った２回のワークショップなどをふまえた、研究の現状を『広島“黒い雨”放射能研究会』としてまとめたものである。言うまでもないことだが、原稿の中味についての責任はそれぞれの著者にあり、研究会として何かの結論を出したりするものではない。

広島市には、検討会の開催、土壌サンプリングの便宜など物心両面でお世話になっている。とりわけ健康福祉局の岡田さんの熱意が私たちを後押ししてきた。広島市役所の関係者のみなさん、また土壌サンプリングに協力して頂いた黒い雨地域の方々に、改めて感謝の意を表しておきたい。

2010年5月

今中　哲二

広島“黒い雨”放射能研究会　世話人